arXiv:cond-mat/0411516v3 [cond-mat.str-el] 23 Feb 2006

# Local distribution approach to disordered binary alloys

A. Alvermann[1] and H. Fehske[1]

[1]Institut für Physik, Ernst-Moritz-Arndt Universität Greifswald, 17489 Greifswald, Germany

We study the electronic structure of the binary alloy and (quantum) percolation model. Our study is based on a self-consistent scheme for the distribution of local Green functions. We obtain detailed results for the density of states, from which the phase diagram of the binary alloy model is constructed, and discuss the existence of a quantum percolation threshold.

PACS numbers: 71.23.An, 72.80.Ng

## I. INTRODUCTION

Many solids, like alloys or doped semiconductors, form crystals consisting of two or more chemical species. In contrast to amorphous solids they possess, at least approximately, a regular lattice whose sites are randomly occupied by the different components. Understanding their electronic structure is an important task which we will address here through an approach that allows for a comprehensive description of such substitutionally disordered systems. This approach, which we call the local distribution (LD) approach, considers the local density of states (LDOS) $\rho_i(\omega)$, which is a quantity of primary importance in systems with prominent local interactions or scattering, e.g. in the formation of local magnetic moments. What makes the LD approach 'non-standard' is that it directly deals with the *distribution* of the LDOS in the spirit that Anderson introduced in his pioneering work.[1] While the LDOS is directly related to the amplitude of the electron's wave-functions on a certain lattice site, its distribution captures the fluctuations of the wave-functions through the system.

The LD approach has been originally developed for a description of Anderson localization[2], and furthermore been applied to systems with topological disorder.[3,4] In this article we like to demonstrate that it can also describe systems with a bimodal disorder distribution, as the binary alloy model. It has been noted several times (see e.g. Refs. 5,6,7), that the physics of this model is only partially covered in a mean field description as provided by the coherent potential approximation (CPA). Instead one has to account for the specific configuration of atoms in the vicinity of a lattice site.[8,9] To give a better description, a variety of (cluster) extensions to CPA has been devised, which explicitly treat correlations on finite clusters (see e.g. Ref. 6 or Ref. 10). We will show that the LD approach can serve as a conclusive extension of CPA—indeed it contains the CPA as a limit, see App. A—which implicitly contains these correlations.

Besides giving very precise results for non-interacting systems, an appealing feature of the LD approach is its possible application to interacting disordered systems. Recently some progress in this direction has been made using the LD approach in combination with dynamical mean field theory.[11] We could e.g. show that polaron formation in an electron-phonon-coupled system is enhanced in the presence of impurities, leading to polaron like defect states.[12] The Mott transition in a binary alloy is another example, where the LD approach might help to substantiate present results.[13]

The outline of this article is as follows: We will shortly introduce the binary alloy model and the associated distributions, and then apply the LD approach. As a limiting case we will consider the (quantum) percolation model, and finally conclude. The two appendices contain the derivation of the LD approach and its application to the Anderson localization problem.

## II. MODEL AND DISTRIBUTIONS

The simplest model for an electron moving in a crystal with substitutional disorder is given by the Hamiltonian

$$H = \sum_i \epsilon_i c_i^\dagger c_i - t \sum_{\langle i,j \rangle} c_i^\dagger c_j \; , \tag{1}$$

where $t$ denotes the tight-binding hopping integral between nearest neighbour sites on a given lattice, and the $\epsilon_i$'s are random on-site potentials.

The model is further specified through the probability distribution of the random variables $\epsilon_i$. We only consider models where the $\epsilon_i$ are identically independently distributed random variables with a fixed distribution $p(\epsilon_i)$. The Anderson model of localization, the binary alloy model and the quantum percolation model are examples.

For given values of the $\epsilon_i$, i.e. for a specific disorder configuration ('one specimen'), the local density of states (LDOS)

$$\rho_i(\omega) = -\mathrm{Im}\, G_{ii}(\omega)/\pi \tag{2}$$

(expressed through the retarded Green function $G_{ii}(\omega)$) has a definite value on each lattice site $i$. For the ordered system, translational symmetry implies that $\rho_i(\omega)$ has the same value for every $i$. In a disordered system, $\rho_i(\omega)$ varies with $i$, so it takes on different values with a certain probability. The corresponding probability distribution $p(\rho_i, \omega)$ captures the fluctuation of the LDOS through the system. It is reasonable to assume that for an infinite system $p(\rho_i, \omega)$ does not depend on the explicit values of the $\epsilon_i$, but only on the probability distribution $p(\epsilon_i)$. We thus assume that the distribution $p(\rho_i, \omega)$ is, in a slight 'abuse of language', self-averaging: It does not depend on the specific disorder configuration looked at, but takes on a definite value in the thermodynamic limit. Moreover $p(\rho_i, \omega)$ has a second meaning. If we look at a fixed lattice site $i$ but consider all possible values of the $\epsilon_i$, the LDOS is a random variable in its own right, whose probability distribution is equal to $p(\rho_i, \omega)$ as defined above. So $p(\rho_i, \omega)$ gives (i) the probability that the LDOS has a certain value on some lattice site, when all $\epsilon_i$ are fixed, and (ii) the probability that the LDOS has a certain value on a fixed lattice site $i$, when the $\epsilon_i$ vary. Note that $p(\rho_i, \omega)$ does not depend on $i$, in contrast to $\rho_i(\omega)$.

One basic physical quantity that is calculated from $p(\rho_i, \omega)$ is the *arithmetically averaged density of states* (DOS)

$$\rho(\omega) = \int_0^\infty \rho_i \, p(\rho_i, \omega) \, d\rho_i \tag{3}$$

which counts the number of states at energy $\omega$. For the ordered system, when $\rho_i(\omega)$ does not depend on $i$, $p(\rho_i, \omega) = \delta(\rho_i - \rho(\omega))$ is a $\delta$-peak at the DOS. In the presence of disorder $p(\rho_i, \omega)$ attains a certain width and provides additional information on the character of the electronic states in the system. A narrow distribution corresponds to more or less homogeneous states, when electron scattering is weak, while a broad distribution reflects strong scattering leading to very inhomogeneous states. The essential information on the character of states at energy $\omega$ is thus provided by the distribution $p(\rho_i, \omega)$, which gives a more detailed description of the disordered system than the DOS $\rho(\omega)$ alone.

In particular we can decide whether states at $\omega$ are localized if we employ the precise definition of $p(\rho_i, \omega)$. The retarded Green function $G_{ii}(\omega)$, hence the LDOS and its distribution, is usually calculated for a complex energy $\omega + i\eta$ with a small positive imaginary part $\eta$, followed by analytical continuation to the real axis, i.e. $\eta \to 0$. A finite $\eta$ gives a Lorentzian broadening with respect to $\omega$, i.e. a finite energy resolution. For $\eta \to 0$, the resolution increases until peaks in the LDOS (corresponding to poles of $G_{ii}(\omega)$) and bands (corresponding to branch cuts of $G_{ii}(\omega)$) can be separated. The behaviour of the distribution in the limit $\eta \to 0$ is thus different depending on the spectral properties of the system. For a spectrum consisting only of discrete peaks—this corresponds to localized states—the distribution becomes singular for $\eta \to 0$. Contrary to this we get a regular distribution if the spectrum is continuous as for extended band ('Bloch') states. We use this property in the study of Anderson localization (see App. B), and will use it for the fragmented spectra of the quantum percolation model.

In this article we obtain $p(\rho_i, \omega)$ directly through the LD approach (for details see App. A). It is natural to compare the results for $\rho(\omega)$ of the LD approach to the corresponding CPA results. While the lattice enters the CPA calculations only through the lattice DOS for the ordered system the LD approach is explicitly constructed for a Bethe lattice[22]. Owing to the absence of loops the Bethe lattice is a kind of mean-field approximation to (hyper-) cubic lattices. Its particular geometry does not affect the qualitative behaviour away from the localization transition, which indeed is similar to a cubic lattice in three dimensions, see e.g. our discussion of the quantum percolation model (Sec. V) or the phase diagram obtained for the Anderson model (App. B). Conversely the existence of different phases and transitions in between is correctly described by the LD approach for dimensions $\geq 3$, similar to the success of dynamical mean field theory for interacting systems in high dimensions. Of course at the phase transition, when the correlation length diverges, results for Bethe and cubic lattices differ (see Ref. 14 and App. B). Weak localization in two dimensions, on the other hand, is related to interference on closed loops and thus not seen on a Bethe lattice.

## III. BINARY ALLOY MODEL

The binary alloy model has a bimodal disorder distribution

$$p(\epsilon_i) = c_A \delta(\epsilon_i - E_A) + (1 - c_A) \delta(\epsilon_i - E_B) \quad , \tag{4}$$

corresponding to a crystal randomly composed of A-atoms (B-atoms) at energy $E_A$ ($E_B$). We set $E_A = -\Delta/2$, $E_B = \Delta/2$, i.e. $\Delta = E_B - E_A$. Different aspects of the involved physics of the binary alloy model have been discussed previously (see e.g. Refs. 5,6,7,8,9). The local electron motion strongly depends on the configuration of atoms at (and in the vicinity of) a certain lattice site. This 'cluster effect', showing up as peaks in the DOS, is not obtained by the CPA. We will show that the LD approach can give a (more) complete picture with fair ease. Especially the DOS becomes accessible and will turn out to be important for a thorough understanding.

### A. Low A-concentration – small separation energy

We first study the situation of low concentration $c_A = 0.1$ of A-atoms (which is below the classical percolation threshold, cf. Sec. V). The A-atoms can be considered as the minority species in a bulk system of B-atoms (doping a semiconductor is an example).

For small separation energy $\Delta = 0.3$ the energy levels of the minority A-atoms lie inside the B-band. The DOS mainly consists of the B-band centered at $E_B = +0.15$, but shows some additional structures at the lower band edge, which are absent in the CPA DOS (cf. Fig. 1). They originate from the strong fluctuations in the local environment of an atom, which can be clearly seen in the distribution of the LDOS (cf. Fig. 1). Note the various

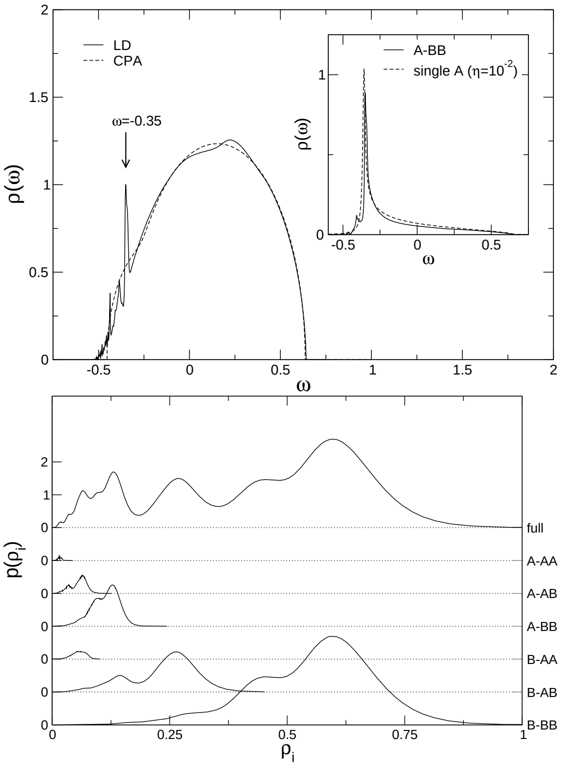

FIG. 1: Binary alloy with $\Delta = 0.3$, $c_A = 0.1$. The upper panel shows the DOS, obtained within the LD approach and CPA. The inset displays the conditional DOS for the cluster configuration $A - BB$, the dashed curve has been calculated using Eq. (5) with broadening $\eta = 10^{-2}$ (see text). The lower panel shows the distribution of the LDOS at $\omega = 0.6$ (curve on top). The six other curves show the distribution of the conditional LDOS for a specified cluster of three sites.

peaks of this distribution (in contrast to the Anderson model, see App. B), and its large width displaying the pronounced fluctuations of the electron's wave-functions.

To understand the consequences of different atoms situated at a lattice site we can look at the 'conditional' LDOS $\rho_i^{A/B}(\omega)$, subject to the constraint that an $A$- respectively $B$-atom is located at site $i$. More generally we can specify a certain configuration of atoms on a cluster of sites centered at $i$. By considering larger and larger clusters every peak in the distribution of the conditional LDOS (and in the DOS) can be attributed to a specific configuration (cf. Fig. 1). As the simplest example the pronounced peak at $\omega \approx -0.35$ results from a single A-atom surrounded by B-atoms (cf. inset Fig. 1). Its approximate position and form follow from the simple formula

$$G_A(\omega) = \left[ \frac{\omega + E_B}{2} - E_A + \sqrt{\left(\frac{\omega - E_B}{2}\right)^2 - \frac{W^2}{16}} \right]^{-1} \tag{5}$$

for the local Green function of one A-impurity embedded in a B-lattice. The corresponding DOS, using a Lorentzian broadening $\eta = 0.02$ in the energy argument $\omega + \mathrm{i}\eta$ of the Green function to mimic the effect of tunnelling between different A-atoms, fits the conditional DOS very well (dashed curve in inset of Fig. 1). The complementary situation of a B-atom surrounded by A-atoms contributes to the 'hump' in the B-band (cf. Fig. 1), which arises from B-atoms neighbouring to A-atoms.

It should be noted that Eq. (5) gives a $\delta$-peak outside the B-band, corresponding to the impurity state at the A-atom, only above a critical value of $\Delta$. This is another evidence that the Bethe lattice should be understood as an approximation to lattices in dimensions $d \geq 3$.

### B. Low A-concentration – split band case

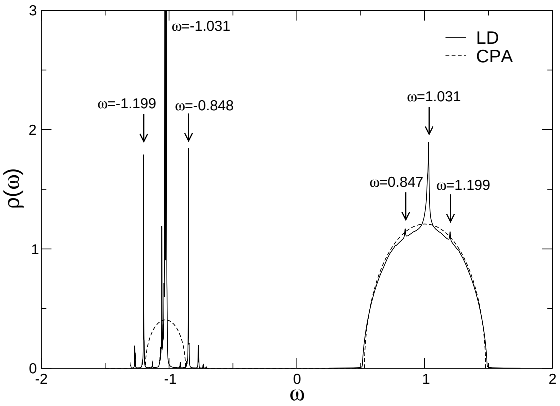

FIG. 2: DOS for the binary alloy with $\Delta = 2.0$, $c_A = 0.1$. To broaden the peaks of the 'A-states' we add an artificial imaginary part $\eta = 10^{-3}$ to the energy argument $\omega$ of the Green function $G_{ii}(\omega)$ in Eq. (2). Arrows mark the position of three peaks each in the A- and B-band.

Increasing the separation energy to $\Delta = 2.0$ (still with $c_A = 0.1$) leads to the split band case (see Fig. 2). The majority B-atoms still form a band whose DOS shows some additional spikes.

The concentration of the minority A-atoms is below the classical percolation threshold hence only finite A-clusters exist (cf. Sec. V). Due to the large energy separation the 'A-states' on these clusters are strongly damped through scattering on B-atoms. Accordingly the 'A-states' do not form a band of (extended) states but a fragmented set of peaks with varying height and width, reminiscent of the percolation model (cf. Sec. V). Again these peaks emerge from A-clusters embedded in the B-lattice. The central peak at $\omega = -1.031$ whose position can be again calculated with Eq. (5) corresponds to a single A-atom surrounded by B-atoms. Similarly the two side peaks result from two adjacent A-atoms, and so forth. The weight of these peaks decreases exponentially as $c_A^N$ for a $N$-atomic cluster. The complementary configurations, reversing the role of A- and B-atoms, yield spikes in the B-band. Since the concentration of B-atoms is large these spikes do not form peaks but merge with the B-band.

Owing to the different strength of scattering we expect that all ‘A-states’ are localized, while the ‘B-band’ remains extended. In accordance with localization in the Anderson model (App. B) we can extract the nature of states from the behaviour of the distribution $p(\rho_i, \omega)$ for $\omega$ shifted by a small imaginary part $\eta$. Indeed we find that, for $\eta \to 0$, the distribution is singular in the energy range of the ‘A-states’ but regular for the B-band, which proves that ‘A-states’ are localized and the ‘B-band’ remains extended.

### C. Phase diagram

In Fig. 3 we show the phase diagram of the binary alloy for low concentration $c_A = 0.1$. For $\Delta$ below a critical value $\Delta_c \approx 0.5$ the spectrum consists of a single band, which splits into two bands above $\Delta_c$. The value of $\Delta_c$ is a little bit larger than obtained within CPA ($\Delta_c^{\mathrm{CPA}} \approx 0.45$), but significantly smaller than $\Delta = 1$, when two bands with bandwidth $W = 1$ centered around $\pm\Delta/2$ would no longer overlap.

The phase diagram shows the rich physics of the binary alloy As discussed in the previous two sections: (i) formation of many gaps, leading to a strongly fragmented minority ‘band’, (ii) the bands between the gaps show additional spikes, (iii) for split bands and low concentrations, minority states are localized impurity states, while majority states are extended band states. These three important effects go beyond the CPA, which gives only the band splitting. The CPA works reasonably well for the majority band, where the local environment of a lattice site is less important, but it cannot describe the fine structure of the minority band in even a crude way. These findings are in full agreement with Ref. 7, and we can additionally show the exact form of the DOS which is one outcome of the LD approach. So far we have dealt with a low concentration $c_A$ of the A-species below the classical percolation threshold $p_c = 1/K$ for the Bethe lattice. Then, when only finite A-clusters exist, strong signatures and fragmentation of the DOS could be observed. Increasing $K$ with $c_A$ fixed, these signatures are partially weakened as long as $c_A < p_c$ (see Fig. 4). Above the percolation threshold ($c_A > p_c$), infinite A-clusters exist, leading to a band which is no longer fragmented. Nevertheless the DOS still has peaks. For large $K$ (equivalent to $p_c \ll c_A$) the DOS approaches a semicircular form, anticipating the CPA result in the limit $K = \infty$ (cf. the discussion in the appendices).

For equal concentration $c_A = c_B = 0.5$ and $K = 3$, both atom species are in the percolating regime, which corresponds not to a doped material but to a stoichiometric compound. The phase diagram (Fig. 3) shows that the signatures in the DOS become more pronounced with increasing $\Delta$, when the binary alloy model approaches the percolation model (see Sec. V).

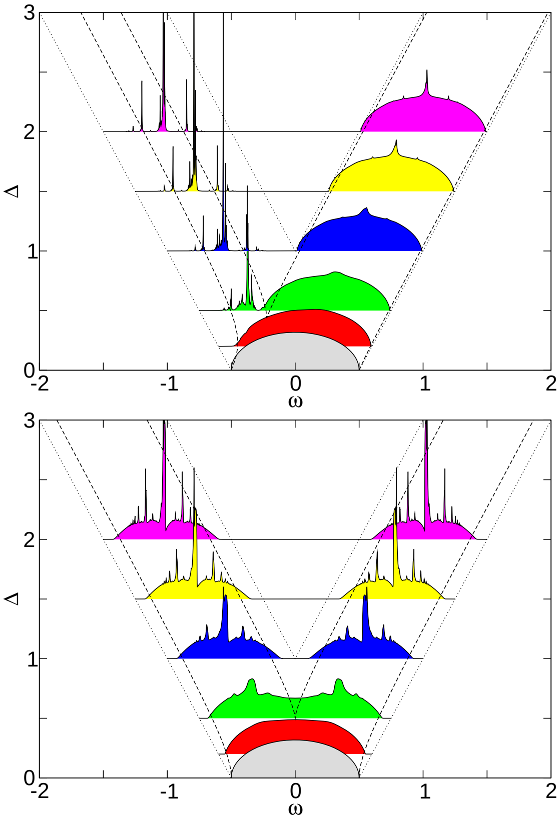

FIG. 3: (Colour online) Phase diagram of the binary alloy, for low concentration $c_A = 0.1$ (upper panel), and equal concentration $c_A = c_B = 0.5$ (lower panel). The solid filled curves show the DOS for various $\Delta$. The dashed curves show the CPA band edges, and the dotted lines mark $\omega = \pm\Delta/2 \pm W/2$.

## IV. COMBINED ANDERSON AND BINARY ALLOY MODEL

The binary alloy model shows a distinct tendency towards peak and gap formation. This behaviour is a generic feature of systems with a bimodal disorder distribution. For example consider the binary alloy model with additional on-site box disorder $\gamma$, i.e.

$$p(\epsilon_i) = \frac{c_A}{\gamma}\Theta(\gamma/2 - |\epsilon_i - E_A|) + \frac{1 - c_A}{\gamma}\Theta(\gamma/2 - |\epsilon_i - E_B|) \,. \tag{6}$$

The CPA suggests that the system is the combination of two rescaled Anderson models. This is consistent with its phase diagram concerning the position of mobility edges.[15] The LD approach additionally shows that structures similar to the ‘pure’ binary alloy appear (cf. Fig. 5). Evidently the system is not adequately described in terms of rescaled Anderson models. For the parameters considered $\gamma$ is on the same energy scale as the hopping matrix element $t$ (here $t = W/\sqrt{32}$, i.e. $\gamma \approx 0.56t$). It is thus reasonable to assume that in a real alloy, e.g. a doped semiconductor, the peaked structure of the binary alloy DOS can be found. Furthermore, if we extract local-

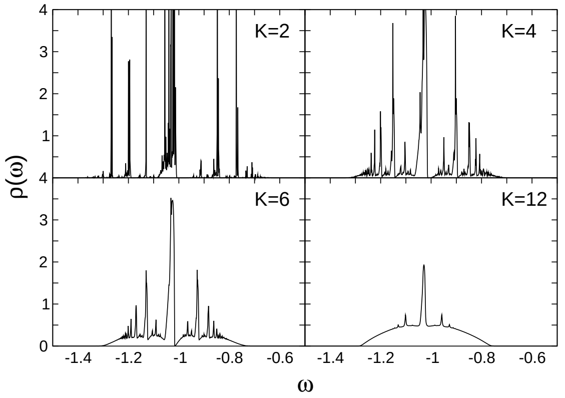

FIG. 4: DOS of the impurity band for $\Delta = 2.0$ and $c_A = 0.2$, with increasing number of nearest neighbours $K$ of the Bethe lattice. For $K = 2, 4$, the concentration $c_A$ is below the classical percolation threshold $p_c = 1/K$, for $K = 6, 12$ above. In contrast to Fig. 2 we did not broaden the peaks with an additional $\eta$.

ization properties of the system by the $\eta \to 0$-limit (cf. App. B), we find the A-band to be entirely localized (see Fig. 5). Nevertheless $\gamma$ is much smaller than the critical disorder ($\gamma_c \simeq 3 \times$ bandwidth) for Anderson localization of the A-subband (in agreement with Ref. 15). Therefore localization of the A-band is increased due to the strong scattering occurring for the minority band in the binary alloy. This suggests that impurity band states in a doped semiconductor will almost always be localized.

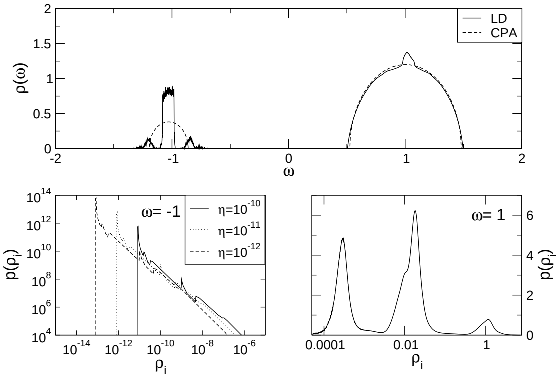

FIG. 5: The upper panel shows the DOS for the binary alloy ($\Delta = 2.0$, $c_A = 0.1$) with additional on-site disorder $\gamma = 0.1$. (see Eq. 6). The bottom row displays the dependence on $\eta$ of the LDOS distribution. Lower left panel: In the center of the A-band at $\omega = -1$ the distribution becomes singular for $\eta \to 0$, i.e. states are localized. Lower right panel: For the B-band at $\omega = +1$ the distribution is independent of $\eta$, and has a peaked structure known from the binary alloy model (cf. Fig. 1).

## V. QUANTUM PERCOLATION MODEL

In the limit $E_B \to \infty$, now keeping $E_A = 0$ fixed, the binary alloy model reduces to the percolation model where A-sites are embedded in an impenetrable host medium[23]. Certainly, in a real alloy with $\Delta < \infty$, the electron has the chance to tunnel through the host barrier. Nevertheless, the percolation model shows very general features which have already shown up in the split band case of the binary alloy model (see above).

Let us first study the DOS. If the concentration $c_A$ of A-atoms is below the classical percolation threshold $p_c$ only finite clusters exist. The corresponding spectrum is a pure point spectrum which densely fills the energy interval $[-W/2, W/2]$ of the tight-binding band ('Dirac comb'). An $N$-site cluster with occurrence probability $c_A^N(1-c_A)^{N+1}$ contributes peaks at energies spread over the full possible range. Consequently the weight of a peak varies in contrast to the Anderson model non-monotonically with $\omega$. Different statistical properties of the finite clusters can be straightforwardly calculated on the Bethe lattice. For instance the weight

$$w_{\text{fin}} = \sum_{N=1}^{\infty} c_A^{N-1}(1-c_A)^{N+1} C_N \tag{7}$$

$$= \begin{cases} 1, & c_A \le 0.5 \\ (1-c_A)^2/c_A^2, & c_A > 0.5 \end{cases} \tag{8}$$

of all finite clusters[24] directly follows by help of the generating function for the Catalan numbers $C_N$, which give the number of binary trees with $N$ sites. For concentrations above $p_c$ ($= 0.5$), when $w_{\text{fin}} < 1$, an infinite percolating cluster exists. This cluster can support extended states which contribute to an continuous spectrum. Since the 'effective' dimension of the percolating cluster is smaller than $K$ (especially close to $p_c$), the bandwidth of the resulting band is smaller than $W$.

The DOS shows strong signatures (peaks and dips), which have already occurred in the binary alloy model (see top picture in Fig. 6). These signatures arise from both isolated finite clusters and finite clusters attached to the backbone of the infinite percolating cluster. With increasing concentration their weight reduces, and the signatures are washed out. At $\omega = 0$ a pronounced $\delta$-peak surrounded by a dip in the DOS exists. With increasing concentration the peak reduces in weight and the dip narrows, eventually both merge to a spike in the band.

The origin of this central peak and the dip can be understood on the same level of reasoning as for Eq. (5). If a single atom is attached to the backbone of the percolating cluster the Green function is modified by the additional hopping to this atom. The DOS then shows a $\delta$-peak at $\omega = 0$, which is the energy of the state located at the atom, and a dip around this peak which arises from damping of states on the percolating cluster. The same argumentation holds for any finite cluster instead of a single atom. Since larger clusters have lower probability

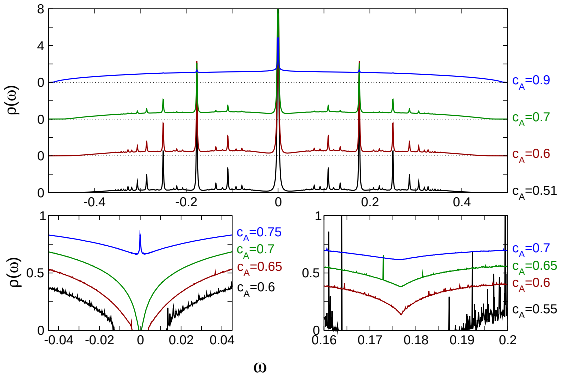

FIG. 6: (Colour online) DOS $\rho(\omega)$ for the percolation model, for various concentrations $c_A$. Upper panel: Full spectrum with Lorentzian broadening $\eta = 10^{-3}$. Lower left panel: Central region around $\omega = 0$ without Lorentzian broadening. Lower right panel: Region around the second peak at $\omega = t = 1/\sqrt{32} \approx 0.177$ without Lorentzian broadening.

of occurrence the central peak is the most pronounced, and exists up to the largest concentrations.

Nevertheless the percolating cluster is not made up of its backbone plus one additional finite cluster, but many finite clusters attached to it. The Green function $G^c(\omega)$ of a (half-)infinite chain with one additional atom attached to each site obeys the recursion relation

$$G^c(\omega) = (\omega - t^2/\omega - t^2 G^c(\omega))^{-1} \tag{9}$$

which is solved by $G^c(\omega) = G^0(\omega - t^2/\omega)$, where $G^0(\omega)$ is the Green function of the Bethe lattice. Of course $G^c(\omega = 0) = 0$ as before, but the diverging real part of $1/\omega$ produces not a dip but a *gap* in the DOS around $\omega = 0$. The validity of this simple argumentation can be tested within the LD approach since its energy resolution is not limited by finite size effects. Without Lorentzian broadening, i.e. $\eta \to 0$, the $\delta$-peaks arising from finite cluster states do not contribute to the DOS (cf. Sec. II), and only the continuous spectrum from extended band states survives. This spectrum indeed shows a gap around $\omega = 0$ for sufficiently small concentrations (cf. Fig. 6, bottom left). Lowering the concentration, gaps open at the energies corresponding to any finite cluster eigenstate. The first additional gaps open at $\omega = \pm t$ (Fig. 6, bottom right), corresponding to two site clusters, which have the second largest weight among all finite clusters. These gaps are filled by peaks from the dense spectrum of finite cluster states, thus are absent in the DOS for any finite energy resolution (cf. Ref. 16). The formation of gaps—which is a kind of ‘level repulsion’—is a significant quantum feature with no counterpart in the classical model.

Besides the DOS the nature of states is important. For concentrations $c_A < p_c$, when only finite clusters exist, all states are localized and no electron transport is possible. For concentrations above $p_c$ a classical electron can traverse the system along the percolating cluster. But a quantum mechanical electron scatters off all irregularities and is possibly localized. This raises the question of a quantum percolation threshold $p_q$ *above* $p_c$.

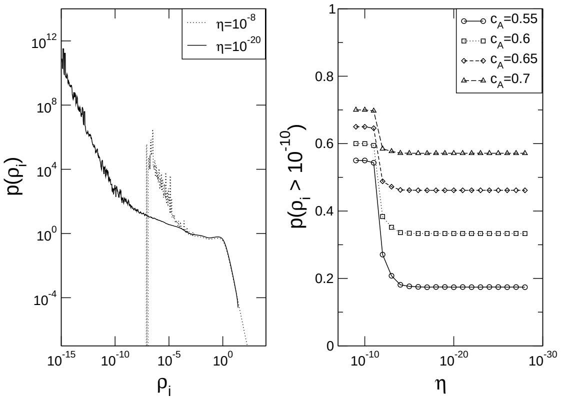

FIG. 7: LDOS distribution for the percolation model at $\omega = 0.1$. Left panel: For $c_A = 0.7$ and two values of regularization $\eta = 10^{-8}$ and $\eta = 10^{-20}$. For $\eta \to 0$ only extended states contribute to $p(\rho_i, \omega)$ at finite $\rho_i$. Right panel: Integrated probability $p(\rho_i > \xi, \omega)$ in dependence on $\eta$, for various $c_A$ and one particular value $\xi = 10^{-10}$. For $c_A \lesssim 0.54$ no states exist at $\omega = 0.1$, and $p(\rho_i, \omega) = 0$.

Close to $p_c$ states on the percolating cluster have only exponentially small weight. It is thus difficult to extract the information about those states from the background of finite cluster contributions. However, we can gain some information from the distribution of the LDOS, if $c_A$ and $\eta$ are varied. Again, if we let $\eta \to 0$, the energy resolution increases until contributions from extended states on the percolating cluster are separated from the discrete peaks of localized states (see left panel of Fig. 7). For fixed energy $\omega$ and suitably large concentration $c_A$ the distribution $p(\rho_i, \omega)$ has finite weight at finite $\rho_i$ in the limit $\eta \to 0$ (see right panel of Fig. 7), which indicates that extended states exist. Their weight can be estimated through the integrated probability $p(\rho_i > \xi, \omega) = \int_\xi^\infty p(\rho_i, \omega)\, d\rho_i$, with $\eta < \xi$. The weight decreases with $c_A$, and abruptly drops to zero at a certain concentration (for $c_A \approx 0.54$ at $\omega = 0.1$). Then no states exist at $\omega$, and $\rho_{\mathrm{ave}}(\omega) = 0$. This behaviour has to be attributed to the fragmentation of the spectrum discussed before. At a given energy $\omega$ a gap will open for concentrations $c_A$ sufficiently close to $p_c$. Before a gap opens at $\omega$, states are extended. After the gap has opened, no states at $\omega$ exist. Between the gaps, which open at different concentrations for different energies, extended states can survive even for very small $c_A$, although all states are extremely damped and practically localized. A definite localization transition from extended to localized states does however not take place, and the only transition occurs when the spectrum is fully fragmented, that is at the classical transition $c_A = p_c$. We conclude, on the basis of these arguments and our numerical results, that, for the percolation problem on the Bethe lattice, a quantum percolation threshold above the classical one does not exist. Note that scattering on the percolating cluster is of a different type than for the Anderson model. The finite clusters attached to the percolating backbone do not act as coherent but incoherent scatterers. So states on the backbone will not be localized for small $c_A$ (i.e. strong scattering), or even immediately localized, as in one dimension.

## VI. CONCLUSIONS

In this article we demonstrated how the LD approach can be used to study localization and percolative effects in alloys. With very moderate computational demands this scheme suffices to resolve the rich structures in the DOS originating from comparably strong disorder fluctuations. Even for the extreme limit of the binary alloy model, the percolation model, convincing results are easily obtained. For instance the question whether gaps form in the percolation model could be definitely answered, and the possibility of a quantum percolation threshold above the classical one could be almost definitely ruled out for the Bethe lattice.

We conclude that the LD approach is a convenient framework for investigations of disorder and localization, and suggest its application to interacting disordered systems.

## APPENDIX A: THE LD APPROACH

The LD approach has been constructed by Abou-Chacra, Anderson, and Thouless[2] on a Bethe lattice. There the local Green function $G_{ii}(\omega) = \langle i|(\omega + \mathrm{i}\eta - H)^{-1}|i\rangle$ can be expressed through Green functions on the $K$ neighbouring lattice sites $j = 1, \ldots, K$,

$$G_{ii}(\omega) = \Big[\omega - \epsilon_i - t^2 \sum_{j=1}^{K} G_{jj}(\omega)\Big]^{-1} \quad , \tag{A1}$$

where each $G_{jj}(\omega)$ on the r.h.s. of this equation is evaluated for the lattice with site $i$ removed. Iterating this expansion an infinite hierarchy of equations is generated ('renormalized perturbation expansion').[17] Instead of solving this hierarchy for many particular realizations of the $\epsilon_i$ and constructing the distribution of $G_{ii}(\omega)$ afterwards the LD approach manages to solve Eq. (A1) directly for the distribution. This solution relies on two properties arising from the special geometry of the Bethe lattice. First, all Green functions in Eq. (A1) correspond to the same geometric situation (one lattice site with $K$ neighbouring sites). Hence their distribution is identical (although their concrete values differ). Moreover, removing site $i$ from the lattice, the lattice sites $j = 1, \ldots, K$ are unconnected, and the $G_{jj}(\omega)$ are independently distributed. Owing to these two properties Eq. (A1) expresses one random variable through $K$ independently distributed random variables with the same distribution, and can therefore be interpreted as a self-consistency equation for the distribution of $G_{ii}(\omega)$.[2,12] Be aware that then the indices $i$, $j$ do not denote specific lattice sites but certain realizations of the random variable $G_{ii}(\omega)$.

For the ordered system ($\epsilon_i = 0$) all Green functions in Eq. (A1) are identical, and the Green function $G^0(\omega) = (8/W^2)(\omega - \sqrt{\omega^2 - W^2/4})$ of the Bethe lattice[17], with bandwidth $W = 4t\sqrt{K}$, is obtained. For a disordered system the solution of Eq. (A1) is obtained through a Monte-Carlo procedure (Gibbs sampling). The distribution is represented through a sample of typically $10^4$ up to $10^7$ elements, depending on the respective case studied. At each step of iteration a new sample is constructed whose elements are calculated through Eq. (A1) with a randomly chosen $\epsilon_i$ and $K$ elements drawn from the previous sample. A hundred up to some thousand iterations are necessary to guarantee convergence. The resulting computation time on a standard desktop PC ranges from few minutes to some hours.

The LD approach comprises the coherent potential approximation (CPA) in the limit of infinite coordination number $K = \infty$. Taking into account the scaling $t \propto 1/\sqrt{K}$ of the hopping matrix element, the sum over $j$ in Eq. (A1) can—assuming the central limit theorem to be applicable—be replaced by the arithmetic average of $G_{jj}$, and the CPA is recovered.

In course of its construction the LD approach works on an infinite lattice (no boundaries, no finite size effects, no finite energy resolution). In the numerical solution the size of the sample determines the resolution which the distribution is sampled with. The resolution can be easily enhanced by increasing the sample size (see below).

## APPENDIX B: ANDERSON MODEL

We describe in this appendix the application of the LD approach to the Anderson localization problem. Although this is not the main objective of this article, it will help to underline the generality of the LD approach.

The Anderson model—which is the prototype model showing a localization transition—is given by Eq. (1) for a uniform distribution of $\epsilon_i$ in the interval $[-\gamma/2, \gamma/2]$,

$$p(\epsilon_i) = \frac{1}{\gamma} \Theta\left(\frac{\gamma}{2} - |\epsilon_i|\right) \quad . \tag{B1}$$

The characteristics of localization show up in $p(\rho_i, \omega)$ (cf. Fig. (8)). Impurity scattering causes the distribution to be strongly asymmetric and broad even for extended states. As one consequence the DOS $\rho(\omega)$ is on a different scale than 'typical' values of the distribution, e.g. the most probable value. On approaching the localization transition the asymmetry further increases. Much weight is transferred to large values of $\rho_i$, while the 'typical' values tends to zero.

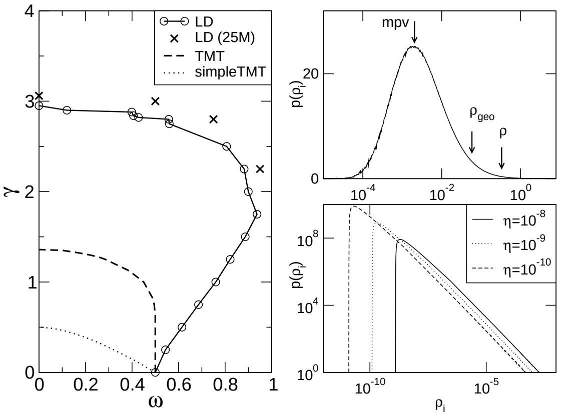

FIG. 8: Left panel: Phase diagram of the Anderson model. The solid (dashed, dotted) curve shows the mobility edge trajectory calculated within the LD approach (TMT, simplified TMT) by means of the $\eta \to 0$ limit, using a sample with $5 \times 10^4$ elements. The crosses indicate points in the $(\omega, \gamma)$-plane corresponding to the mobility edge position for an extremely large sample of $2.5 \times 10^7$ elements. Upper right panel: probability distribution of LDOS for extended states, at $\gamma = 1.5$, $\omega = 0.0$. The distribution is – for not too large values of $\eta$ – independent of $\eta$, but the most probable value ('mpv') is some orders of magnitude smaller than the (geometric) DOS $\rho(\omega)$ ($\rho_{\text{geo}}(\omega)$). Lower right panel: probability distribution $p(\rho_i, \omega)$ for localized states, at $\gamma = 1.5$, $\omega = 0.9$, and three values of $\eta$.

A closer look at the distribution reveals that near the localization transition it shows a power law behaviour over a wide range of $\rho_i$, with an exponent $\simeq 1.45$, which is reasonably close to analytical results obtained from field theoretical considerations.[14]

Passing the localization transition the distribution becomes singular, corresponding to a transition from continuous to discrete spectrum. This characteristic change reflects itself most clearly in the dependence of the distribution on the $\eta$-regularization, when $G_{ii}(\omega)$ is calculated for a complex energy argument $\omega + i\eta$. While the distribution for extended states is stable when decreasing $\eta$, the relevant scale for localized states is entirely set through $\eta$, and the distribution becomes singular for $\eta \to 0$ (see Fig. 8). We can use this different behaviour as a localization criterion, if we perform the $\eta \to 0$ limit numerically. This criterion does not depend on any a priori choice or approximation, hence should be considered 'numerically exact'. As we have already mentioned (cf. App. A) the finite size of the Monte-Carlo sample sets the resolution for sampling $p(\rho_i, \omega)$. If the sample is too small (and thus the resolution too low) an almost singular distribution will be falsely detected as singular while a larger sample correctly gives a regular distribution corresponding to extended states. Accordingly the mobility edge is shifted to larger values of disorder on increasing the sample size (Fig. 8). However, the points on the mobility edge trajectory readily stabilize if the sample is chosen large enough, and a precise determination of the mobility edge is possible.

The LD approach phase diagram for the Anderson model which is then obtained shows the characteristic features of the localization problem in three dimensions.[18,19] These can be most simply understood to arise from the interplay of two competing effects: While, for small disorder, tunnelling between shallow impurities produces extended states outside the tight-binding band, strong scattering on deep impurities takes place with increasing disorder, starting to localize formerly extended states. Therefore a reentrant behaviour of the mobility edge trajectory and the existence of a critical disorder $\gamma_c$ ($\gamma_c \approx 3.0$ for $K = 2$ neighbour sites of the Bethe lattice) for complete localization of all states is found.

According to the mean-field type of approximation, the critical disorder $\gamma_c$ for the Bethe lattice is larger than for a cubic lattice. For $K \to \infty$, $\gamma_c$ grows without bound, i.e. localization is absent in $K = \infty$ (where the LD approach reduces to the CPA). For $K = 1$ the Bethe lattice is a one-dimensional chain, where all states are known to be localized for arbitrary disorder. The sum in Eq. (A1) then contains only one $G_{jj}(\omega)$, which implies that the LD sampling scheme cannot converge to a stable distribution, since different elements of the sample never become related to each other during the sampling. This instability expresses the particular one-dimensional localization behaviour.

For comparison to the LD approach we show in Fig. 8 the mobility edge trajectory obtained within a recently proposed mean-field like approach to Anderson localization, the so-called typical medium theory (TMT).[20,21] This TMT modifies the CPA by reformulating its self-consistency condition in terms of the geometrically averaged DOS

$$\rho_{\text{geo}}(\omega) = \exp\left( \int_0^\infty (\ln \rho_i) p(\rho_i, \omega) d\rho_i \right) \quad . \tag{B2}$$

This average is known to be critical at the localization transition, since it puts much weight at low values of $\rho_i$. It nevertheless does not approximate the 'typical' values, see Fig. 8.

If we compare the lines of vanishing $\rho_{\text{geo}}(\omega)$ from TMT (i.e. the 'TMT mobility edges') with the LD approach phase diagram we see the consequences of this modification: (i) the critical disorder predicted is significantly smaller, and (ii) the reentrant behaviour of the mobility edge is entirely missed.

Remember that the CPA is obtained in the well defined limit of infinite coordination number $K = \infty$, therefore is a controlled approximation. In the TMT construction some ambiguity enters in the choice of the average used. In fact TMT can be further simplified, replacing $\rho_{\text{geo}}(\omega)$ by $\rho_{\text{simp}} = \min\{\rho_i(\epsilon_i = \gamma/2), \rho_i(\epsilon_i = -\gamma/2)\}$. This 'averaging procedure' drastically overestimates the strength of impurity scattering, and the 'simplified TMT' is surely far away from any reasonable description of the underlying physics. However, the phase diagram obtained is very similar to the TMT one. Of course the critical disorder has to be even smaller than in TMT.

Apparently TMT captures strong impurity scattering which is partially neglected in the CPA. However, Anderson localization is not merely a result of strong scattering but quantum interference due to coherent scattering. The similarity between the TMT and 'simplified TMT' results indicates that TMT might not adequately include these interference effects.

---

[1] P. W. Anderson, Physical Review **109**, 1492 (1958).

[2] R. Abou-Chacra, P. W. Anderson, and D. J. Thouless, J. Phys. C **6**, 1734 (1973).

[3] D. E. Logan and P. G. Wolynes, Phys. Rev. B **29**, 6560 (1984).

[4] D. E. Logan and P. G. Wolynes, Phys. Rev. B **36**, 4135 (1987).

[5] S. Kirkpatrick and T. P. Eggarter, Phys. Rev. B **72**, 3598 (1972).

[6] I. Takahashi and M. Shimizu, Prog. Theor. Phys. **51**, 1678 (1974).

[7] C. M. Soukoulis, Q. Li, and G. S. Grest, Phys. Rev. B **45**, 7724 (1992).

[8] P. Dean, Proc. Phys. Soc. **73**, 413 (1959).

[9] M. Tsukada, J. Phys. Soc. Japan **26**, 684 (1969).

[10] R. J. Elliott, J. A. Krumhansl, and P. L. Leath, Rev. Mod. Phys. **46**, 465 (1974).

[11] V. Dobrosavljević and G. Kotliar, Phil. Trans. R. Soc. Lond. A **356**, 57 (1998).

[12] F. X. Bronold, A. Alvermann, and H. Fehske, Phil. Mag. **84**, 673 (2004).

[13] K. Byczuk, W. Hofstetter, and D. Vollhardt, Phys. Rev. B **69**, 045112 (2004).

[14] A. D. Mirlin and Y. V. Fyodorov, Phys. Rev. Lett. **72**, 526 (1994).

[15] I. V. Plyushchay, R. A. Römer, and M. Schreiber, Phys. Rev. B **68**, 064201 (2003).

[16] G. Schubert, A. Weiße, and H. Fehske, Phys. Rev. B **71**, 045126 (2005).

[17] E. N. Economou, *Green's Functions in Quantum Physics*, Springer-Verlag, Berlin, 1983.

[18] B. Kramer and A. MacKinnon, Rep. Prog. Phys. **56**, 1469 (1993).

[19] G. Schubert, A. Weiße, G. Wellein, and H. Fehske, in *High Performance Computing in Science and Engineering, Garching 2004*, edited by A. Bode, F. Durst (Springer-Verlag, Berlin, Heidelberg, 2005), pp. 237–250.

[20] V. Dobrosavljević, A. A. Pastor, and B. K. Nikolić, Europhys. Lett. **62**, 76 (2003).

[21] K. Byczuk, W. Hofstetter, and D. Vollhardt, Phys. Rev. Lett. **94**, 056404 (2005).

[22] The (half-infinite) Bethe lattice is a loop-free tree with a semicircular DOS $\rho(\omega) = (4/\pi W^2)\sqrt{W^2 - 4\omega^2}$.[17] If not stated otherwise, we use a Bethe lattice with $K = 2$ nearest neighbours to any lattice site. The hopping matrix element $t$ is chosen to give a full bandwidth $W = 4t\sqrt{K} = 1$, so energies will be measured in units of $W$.

[23] On the Bethe lattice site and bond percolation are equivalent.

[24] Again on a Bethe lattice with coordination number $K = 2$, cf. first footnote.